



This is a repository copy of *Laser cladding of rail; the effects of depositing material on lower rail grades*.

White Rose Research Online URL for this paper:
<http://eprints.whiterose.ac.uk/154408/>

Version: Accepted Version

Article:

Lu, P., Lewis, S.R., Fretwell-Smith, S. et al. (3 more authors) (2019) Laser cladding of rail; the effects of depositing material on lower rail grades. *Wear*, 438-439. ISSN 0043-1648

<https://doi.org/10.1016/j.wear.2019.203045>

Article available under the terms of the CC-BY-NC-ND licence
(<https://creativecommons.org/licenses/by-nc-nd/4.0/>).

Reuse

This article is distributed under the terms of the Creative Commons Attribution-NonCommercial-NoDerivs (CC BY-NC-ND) licence. This licence only allows you to download this work and share it with others as long as you credit the authors, but you can't change the article in any way or use it commercially. More information and the full terms of the licence here: <https://creativecommons.org/licenses/>

Takedown

If you consider content in White Rose Research Online to be in breach of UK law, please notify us by emailing eprints@whiterose.ac.uk including the URL of the record and the reason for the withdrawal request.



eprints@whiterose.ac.uk
<https://eprints.whiterose.ac.uk/>

LASER CLADDING OF RAIL; THE EFFECTS OF DEPOSITING MATERIAL ON LOWER RAIL GRADES

P Lu¹, S R Lewis², S Fretwell-Smith², D L Engelberg³, D I Fletcher¹, R Lewis^{1,*}

¹ Department of Mechanical Engineering, University of Sheffield, Mappin Street, Sheffield, S1 3JD, UK

² British Steel, Brigg Road, Scunthorpe, Lincolnshire, DN16 1XA, UK

³ School of Materials, University of Manchester, Oxford Road, Manchester, M13 9PL, UK

* roger.lewis@sheffield.ac.uk

Abstract: This paper presents a study comparing the wear performance of laser clad rails. A grade of martensitic stainless steel (MSS) was deposited on two substrate materials: The European standard grade rail steel R260, and a lower grade rail steel R200. A twin-disc method has been used to simulate the contact of wheel and rail under closely controlled conditions. Although cladding on a lesser grade of rail has an effect on the hardness and wear performance of the clad layer (due to dilution), the resulting wear performance of the clad layer assessed using this approach is still vastly improved over R260 material alone.

Keywords: laser cladding, wheel/rail contact, wear, microstructure, twin-disc testing.

1. Introduction and Background

A major proportion of a train network operational cost is the rail maintenance. The cost of replacement of the worn rail or improvement of the rails tribological properties, corrosion properties and contact fatigue resistance, is significant. Meanwhile network downtime caused by rail maintenance also has a great impact on the disruption to commuters and cargo shipping.

Rail is rolled from a single grade of steel, yet different parts of the rail section require their own operating properties. For example, the rail head requires strong tribological properties while the web and foot are required to be structurally robust. There are two main factors that affect the durability of rail track: wear and rolling contact fatigue (RCF) [1, 2]. Premium grade rail steels are available [3], which have good wear and rolling contact fatigue, RCF, resistance. These premium rails are usually heat treated. This procedure is an additional step during the rail manufacturing process and hence has increased cost. Another common method to alleviate RCF, is to periodically grind the rail head which reduces crack development [4]. Other solutions such as surface treatments by peening, case hardening or surface coating can also enhance the wear and RCF performance of many engineering materials. However, rails are usually rolled in lengths of over 100 metres so incorporating these processes into rail manufacture would be impractical and costly. The maximum shear stress, which is a primary driver of RCF, occurs below the surface of the material for low tractive forces and rises as they increase. Traditional thin surface coatings are not sufficiently thick to prevent damage caused by the sub-surface shear stress at its lowest depth.

In recent research [5-8], laser cladding technology was shown to be an alternative way to improve the durability of rail both in terms of wear and RCF [7, 8]. Laser cladding technology can deposit a wide range of beneficial materials onto a certain area or entire existing rail surface. Instead of rolling the entire rail section with costly premium material, laser cladding allows the deposition of the premium material onto the surface of a standard or cheaper structural base steel. Tests performed in [7, 8] show significantly enhanced performance and durability of rail which had been laser clad. In addition, rail not only consists of straight track, but is also made up of other rail constructed components such as switches and crossings (S&C), insulated block joints (IBJs), check rails and tight radius curves. The related maintenance costs of these components are much greater than that of straight track [9, 10]. The laser cladding process offers the possibility to locally treat those components where they are more prone to damage, leading to new

enhanced components with potentially reduced overall lifetime costs. Laser cladding offers the opportunity of altering certain surfaces of components and constructions to meet each individual requirement.

As mentioned above, resistance to wear and RCF plays two vital roles in the maintenance of a rail network. Anti-wear characteristics are related to the hardness and microstructure of the material, which can be improved with laser cladding technology. For example, Guo et al. [11] investigated the microstructure and tribological properties of a Ni-based laser cladding on stainless steel containing Tungsten-Carbide Nickel (WC-Ni) particles. They found that the hardness of the conventional alloy coatings is greatly improved due to the formation of a new hard WC phase. Guo et al. went on to prove that the wear rate was dramatically reduced after investigating the microstructure of the laser cladding layer (Co-based alloy) on the rail-wheel or rail surface [12]. Wang et al. [13] investigated the effect of the amount of lanthanum oxide (Fe-based alloy), in a laser cladding deposit and they achieved a more refined microstructure, which had a greater RCF resistance without sacrificing the surface hardness. Research on Laser cladding has not only been performed at a scaled model test. Lewis et al. [14] conducted a series of full-scale tests on a rail that had been laser clad with a layer of high performance material. In these tests it was shown that the clad rails not only had decreased the wear rates but also improved the RCF resistance over standard rail.

It can be seen that wear and RCF resistance of laser clad coatings is becoming an important research issue and the current state of the art focuses on characterising the wear and RCF resistance over a wide range of laser clad materials, such as in [11-13, 15-18].

In contrast to the previous laser cladding research, there is little work in investigating the contribution of the substrate material. When the head of a rail is clad with premium material the requirements of the substrate become purely structural and it becomes shielded from damage at the rail surface. Moreover, the migration of peak sub-surface shear stress towards the rail surface under high wheel/rail traction conditions places this particularly damaging stress into the harder clad layer, rather than the more vulnerable bulk material. This is especially beneficial as cyclic shear stress combined with compressive wheel load is responsible for rail plastic damage accumulation and crack initiation by the ratchetting mechanism. This said, it is important to study the interface region where the clad/HAZ/bulk meet as this could be susceptible to fatigue problems. This is better achieved in full-scale tests where it is easier to achieve a peak shear stress in this location. As such the work described in this paper was intended to investigate the usage of different substrate materials, namely R200 and R260, using the same cladding material. This also provides an insight into how the substrate affects the properties of the cladding layer, dilution zone and overall rail durability.

2. Experimental Techniques, Materials and Microstructure

2.1 Experimental apparatus

The wear experiments were carried out using the Sheffield University Rolling Sliding (SUROS) twin-disc test machine [19]. Figure 1 shows a schematic of the SUROS rig and typical discs used. This machine uses a line contact between twin-disc specimens to simulate the normal load and rolling-sliding behaviour at the wheel/rail interface. Two discs with diameters of 47 ± 0.2 mm serve as a rail disc (upper specimen) and a wheel disc (lower specimen). These discs are powered and controlled by an AC motor and a Colchester lathe. The difference of speed of wheel and rail discs is used to control the creep. The slip ratio is defined in Equation 1, where ω and r are the rotational speed and rolling radius of the discs, respectively. The load is applied to the wheel disc by a hydraulic piston and load cell.

$$Slip = \frac{\omega_{wheel} \cdot r_{wheel} - \omega_{rail} \cdot r_{rail}}{\omega_{wheel} \cdot r_{wheel} + \omega_{rail} \cdot r_{rail}} \quad (Eq.1)$$

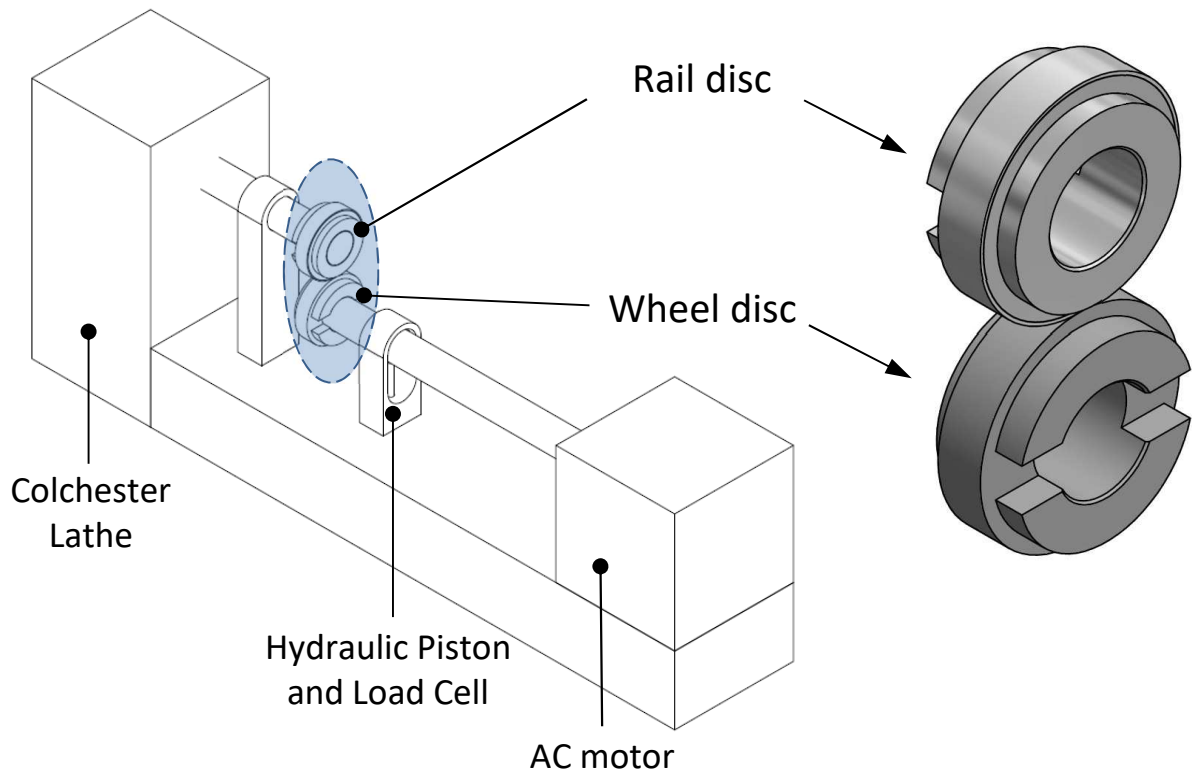


Figure 1. Schematic of the SUROS machine and SUROS wheel & rail disc samples.

2.2 Material

All the wheel and rail disc materials were manufactured from actual wheel and rail. The wheel discs were made from R8 wheel steel. For the rail substrate, two materials were chosen for comparison, R260 and R200, with the properties shown in Table 1, with the original specified hardness converted from Brinell hardness to Vickers hardness. Both rail substrates were machined to cylinders with a diameter of 46 ± 0.2 mm, laser clad, and then machined into SUROS discs.

Table 1. R8 Steel grades & R200 and R260 Steel grades specified by EN.

	Region	Specification	Steel grade	Carbon content	Specified hardness	Specified hardness in HV	Measured hardness
				(% by mass)	(HB)	(HV)	(HV)
Wheel	Europe	EN 13262	ER 8	≤ 0.56	258-296	271-312	275 \pm 10
Rail substrate	Europe	EN 13674-1	R 200	0.4-0.6	200-240	200-252	220 \pm 10
Rail substrate	Europe	EN 13674-1	R 260	0.62-0.8	260-300	274-316	287 \pm 10

The R260 grade material, as the current standard rail material widely used in UK and some other countries in Europe, was chosen to provide representative results for comparison. The lower grade steel substrate R200 is still widely used throughout Europe, however. R200 has some properties which potentially make it an ideal substrate candidate for laser cladding, such as a lower carbon content than R260 (0.4-0.6% compared to 0.62-0.8%) and hence a lower bulk hardness of 200 HB minimum as compared to roughly 260 HB minimum for R260 grade, and better machinability, better weld-ability. Lower rates of foot failure have also been reported which may be due to low residual stresses in the foot or higher fracture toughness [20].

2.3 Laser cladding

In this study, one-step laser cladding by powder injection was employed to clad the rail cylinder specimens. A grade of martensitic stainless steel (MSS) CHROME CORE DN-S (Welding Alloys Group) was used as the cladding material. The composition was attempted to be replicated by powder mixes, yielding the following results: C 0.06; Mn 1.22; Si 0.46; Cr 14.64; Ni 3.31; Mo 0.42; Co 2.01; V 0.51; W 0.62; N 0.04; Al 0.01; S 0.005; P 0.009. This has been found to be less susceptible to ratchetting due to its high hardness and shear yield strength in previous tribological tests [16], was deposited onto the two different grades of rail material. Figure 2(a) shows a schematic of this cladding process, where the high energy laser beam is focused on and scanned across the curved surface of the rail substrate. As the MSS powder passes through the laser it is melted and fuses with the melt pool on the surface of the substrate material. The shaft rotates under the laser to allow a single track of clad to be deposited on the surface. Individual tracks are then overlapped side-by-side to cover the shaft surface. As the laser passes the substrate will start to cool at a rapid rate. This high rate of cooling is due to the greater volume of substrate which is at a lower temperature than the freshly laid deposit. This heating and rapid cooling of the substrate causes changes in its microstructure throughout a certain depth of the bulk, which is called the heat affected zone (HAZ).

Figure 2 (b) gives an example of the cylinders coated by cladding tracks. It should be noted that all the cladding parameters including the MSS powder feeding rate, the laser power and the rotating speed of the shaft were all optimized to achieve a poreless clad layer with outstanding mechanical properties, as well as a satisfactory bond between the substrate and deposit.

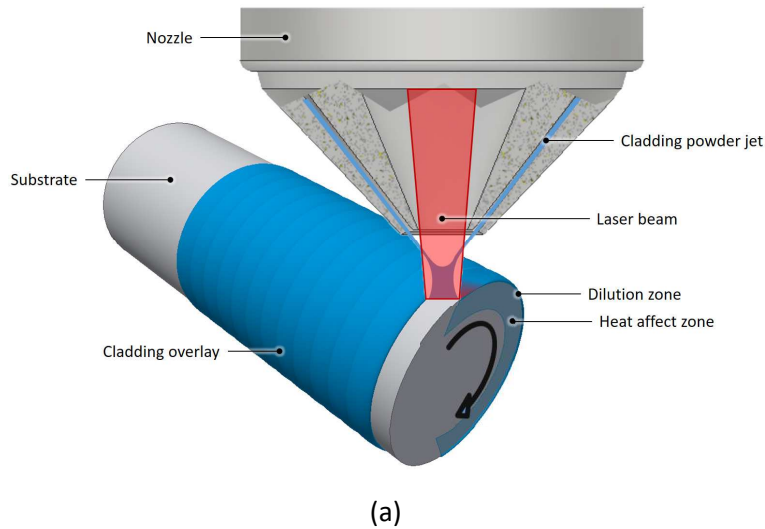


Figure 2. Laser cladding (a) laser cladding scheme (b) laser clad cylinders prior to finish grinding.

Once cooled the clad layer was ground back to give a smooth surface finish which was suitable for testing.

The single layer of MSS material had a mean post-grinding thickness of 1.10 mm. The ground cylinders were then sectioned and machined into SUROS rail specimens with dimensions as shown in Figure 3. The wheel discs were not clad as the focus of this work was the cladding of rails only.

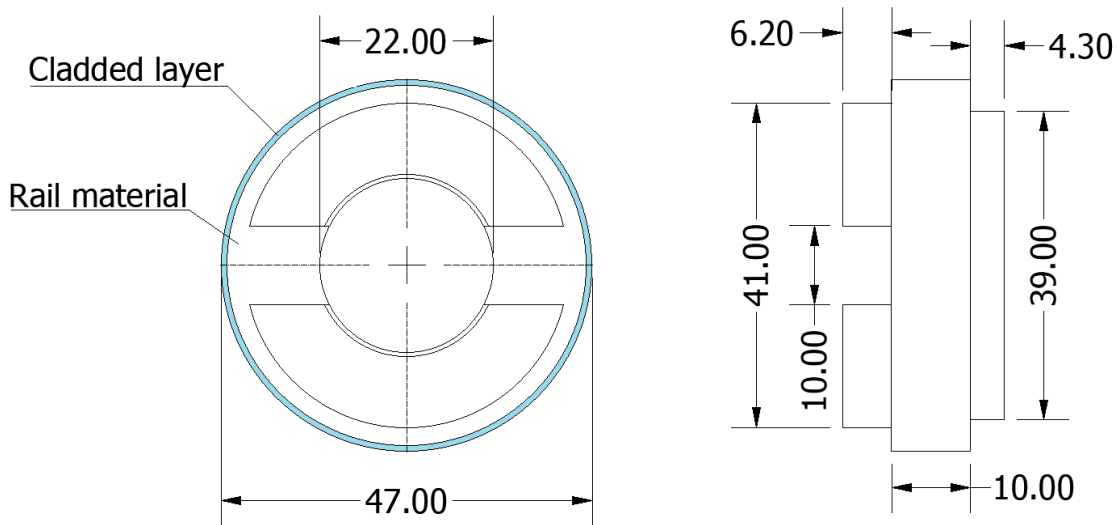


Figure 3. Cladded rail disc parameters.

2.4 Micro-hardness measurements

For microhardness mapping, the discs were sectioned, mounted in Bakelite base and polished for the micro-hardness and microstructural analysis. Pre-test micro-hardness measurements were taken with un-tested discs. These results were generated after cladding, but prior to any load application, so did not capture any strain hardening under load. Vickers micro-hardness measurements were taken using a load of 1.00 kg and dwell time of 10 seconds. The indentation process started from the cladding edge towards the centre of the specimen, and the edge was defined as the zero position, see Fig.4.

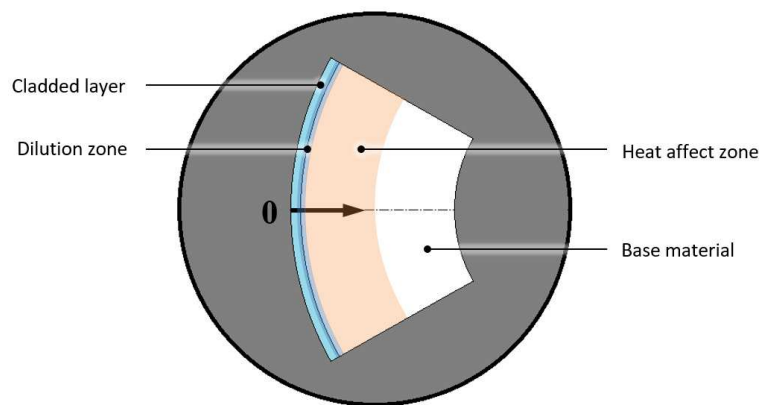


Figure 4. Hardness mapping direction and location.

Figure 5 shows results of microhardness measurements for the R200 and R260 rail material clad with a single layer of MSS material. As shown in Figure 5, the hardness of the MSS clad layer ranges from 530HV for MSS on the R200 steel substrate to 630HV for MSS on the R260 substrate. It can also be seen that the increase of the hardness of the substrate material leads to a corresponding increase in the hardness of the MSS deposit, possibly caused by mixing of the deposit material with the lower (R200) or higher (R260) carbon content substrate during the fusion stage of the cladding process.

The material in the “dilution” zone, where the clad material mixed with the base material, has a hardness value between that of the clad layer and the base material. While in the HAZ, where the base material’s

microstructure is changed during the heating and cooling process, the hardness reduced gradually towards the boundary with the base material. This could be in part due to the fact the grain size changes through the HAZ. Other factors could be related to microstructural changes including partial spheroidisation of cementite lamellae or differences in pearlite spacing.

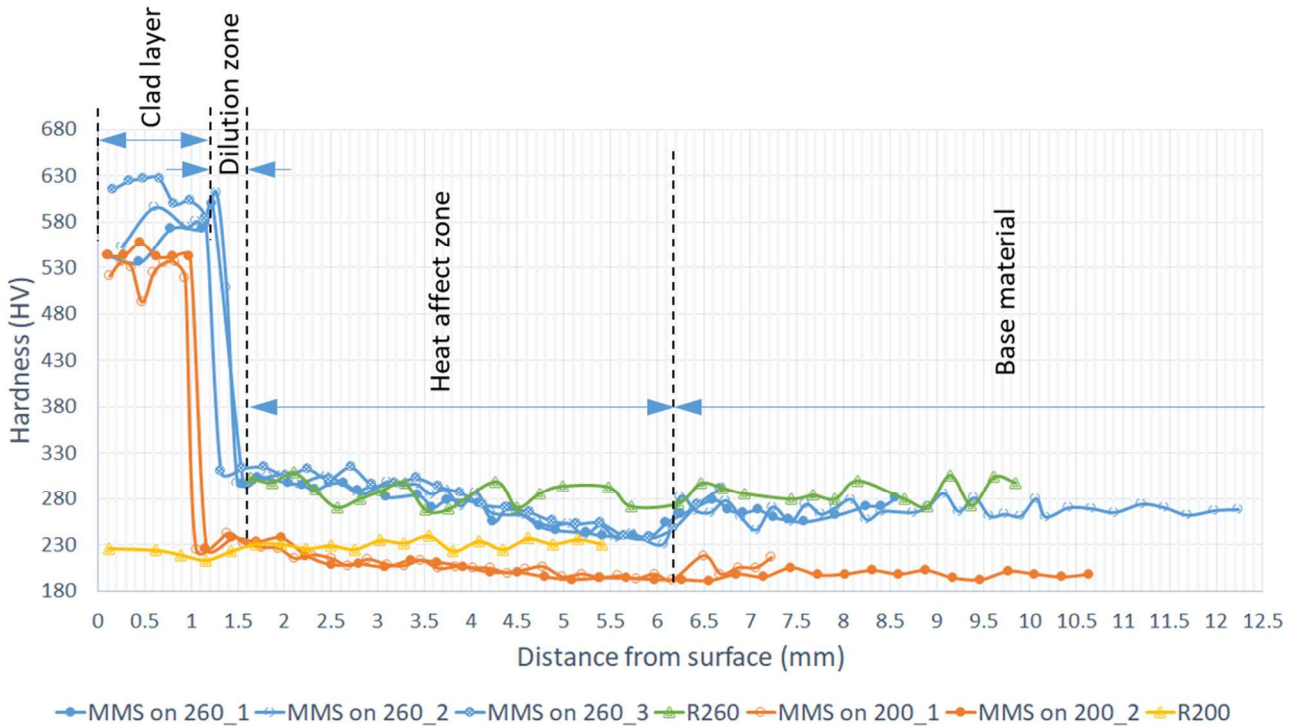


Figure 5. Hardness mapping for all samples before SUROS testing.

2.5 Microstructure analysis

Images of all microstructure are shown in Figures 6 and 7. The heat affected zones (HAZ) were classified according to the term system of Farichild [21]. All polished specimens for microscope and SEM analysis were etched with 2% Nital to expose the microstructural features. For each material, low magnification overview images were taken using an optical microscope CARL ZEISS axio imager a2m (Zeiss Göttingen, Germany). Higher magnification assessment was then carried out via backscattered electron (BSE) SEM analysis by using a Hitachi TM-3030 Tabletop Scanning Electron Microscope (SEM). Images are provided in two magnifications to highlight the difference in microstructure (coarse vs. fine grained) as a function of distance throughout the clad layer. The overview in Figures 6 and 7 show a HAZ dilution zone, coarse grained, and fine grained microstructure zone, followed by an inter-critical and sub-critical HAZ adjacent to the base material of the untested cladding on R260 and R200, respectively.

For the clad layers, the 2% Nital acid solution could not expose microstructural features, therefore a more corrosive solution of 4.76% nitric acid, 47.62% hydrochloric acid in 47.62% water, was used to reveal their microstructure, and the results are shown in Figures 8 and 9 for MSS on R260 and MSS on R200, respectively. It should be noted that the strong etchant caused some local dissolution/attack of additional microstructure constituents, as none of them can be observed from the 2% Nital etched samples shown in Figures 6 and 7. The clad layer is characterised as the clad edge (close to the top side of the cladding), the clad zone, and dilution zone close the substrate HAZ.

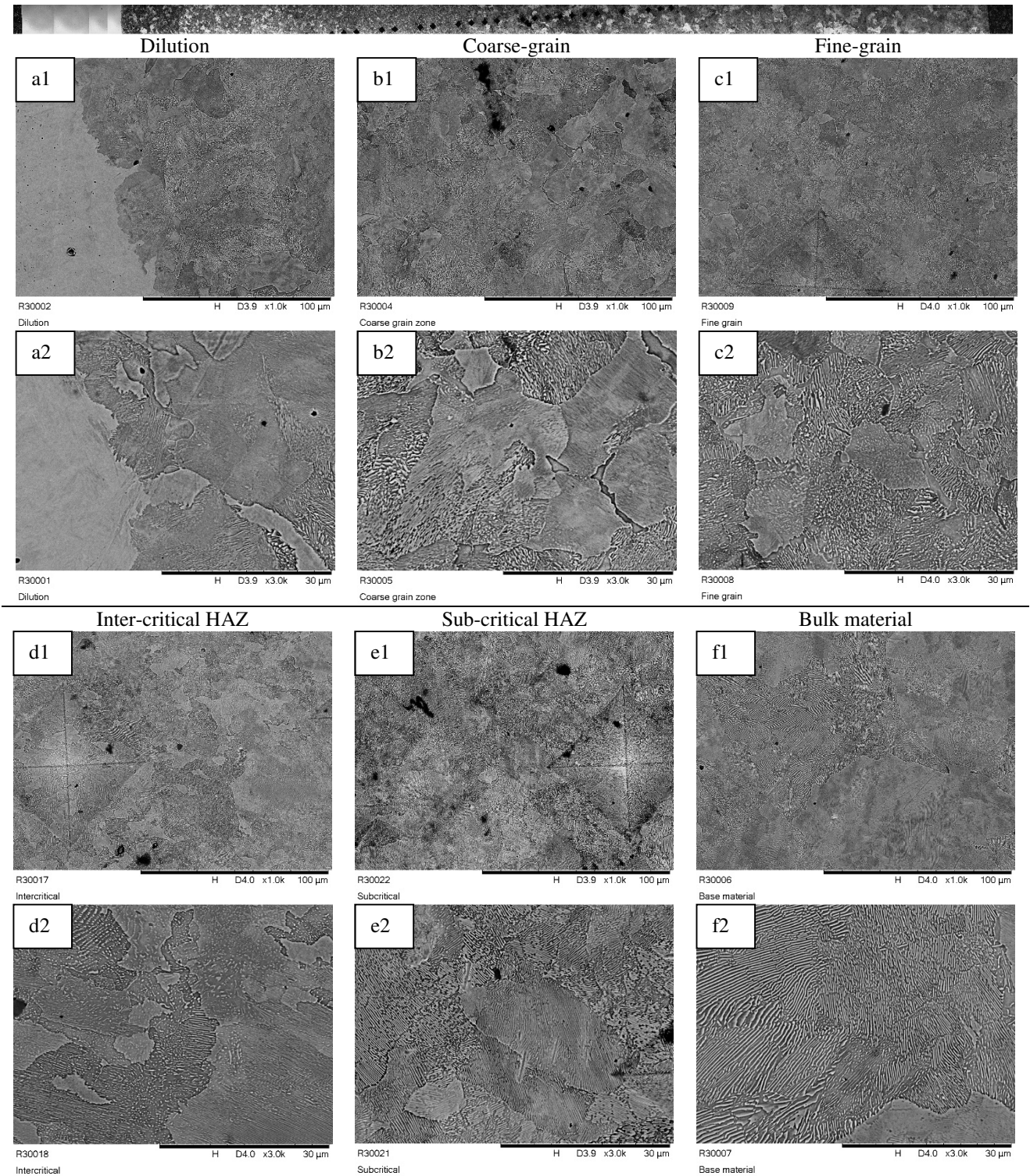


Figure 6. Microstructure of HAZ in untested MMS on R260 (2% Nital etched): (a1), (a2) are for the Dilution zone. (b1), (b2) are for the Coarse-grain. (c1), (c2) are for the Fine-grain zone. (d1), (d2) are for the Inter-critical zone. (e1), (e2) are for the Sub-critical zone. (f1), (f2) are for the Base material.

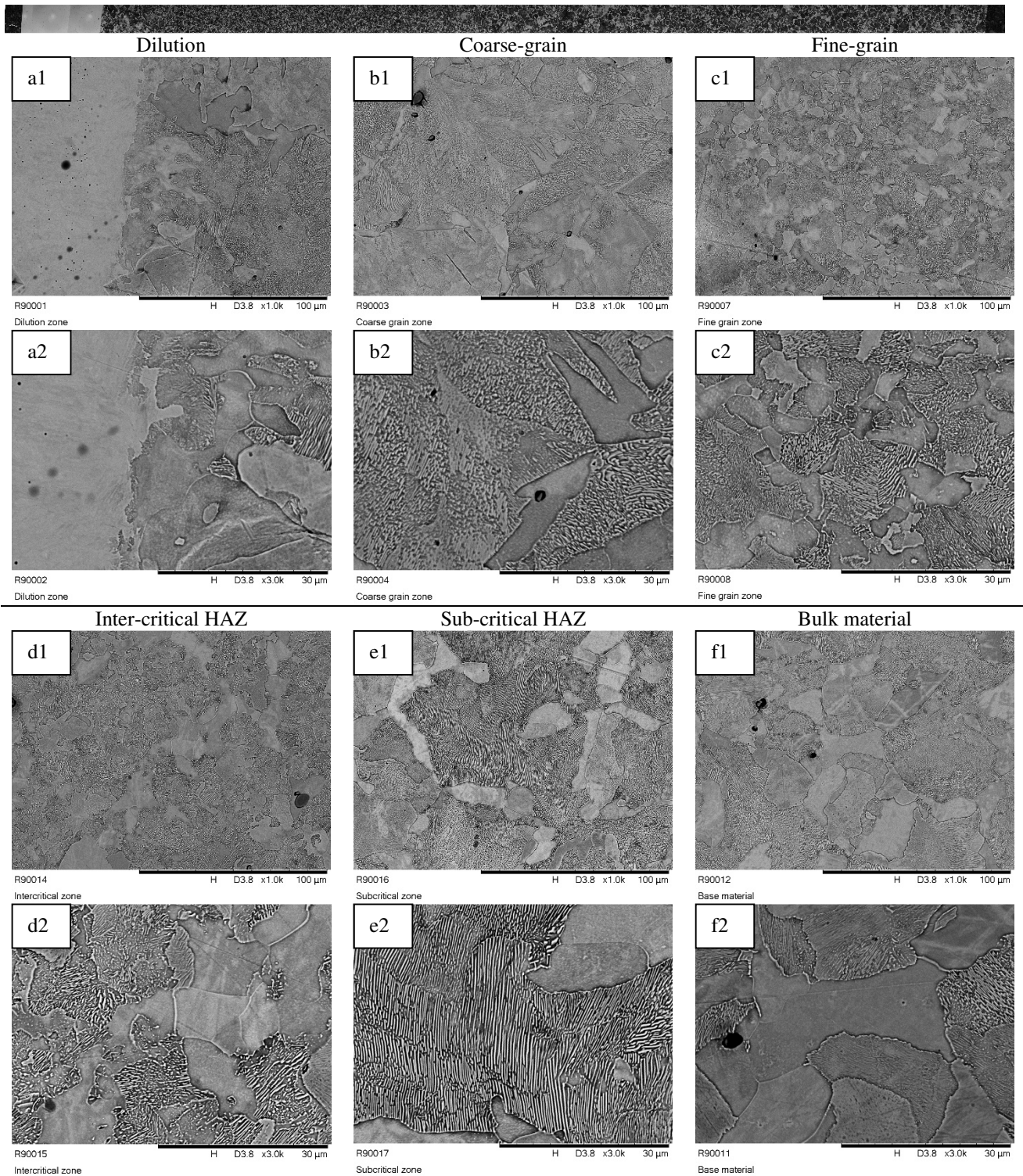


Figure 7. Microstructure of HAZ in untested MMS on R200 (2% Nital etched): (a1), (a2) are for the Dilution zone. (b1), (b2) are for the Coarse-grain. (c1), (c2) are for the Fine-grain zone. (d1), (d2) are for the Inter-critical zone. (e1), (e2) are for the Sub-critical zone. (f1), (f2) are for the Base material.

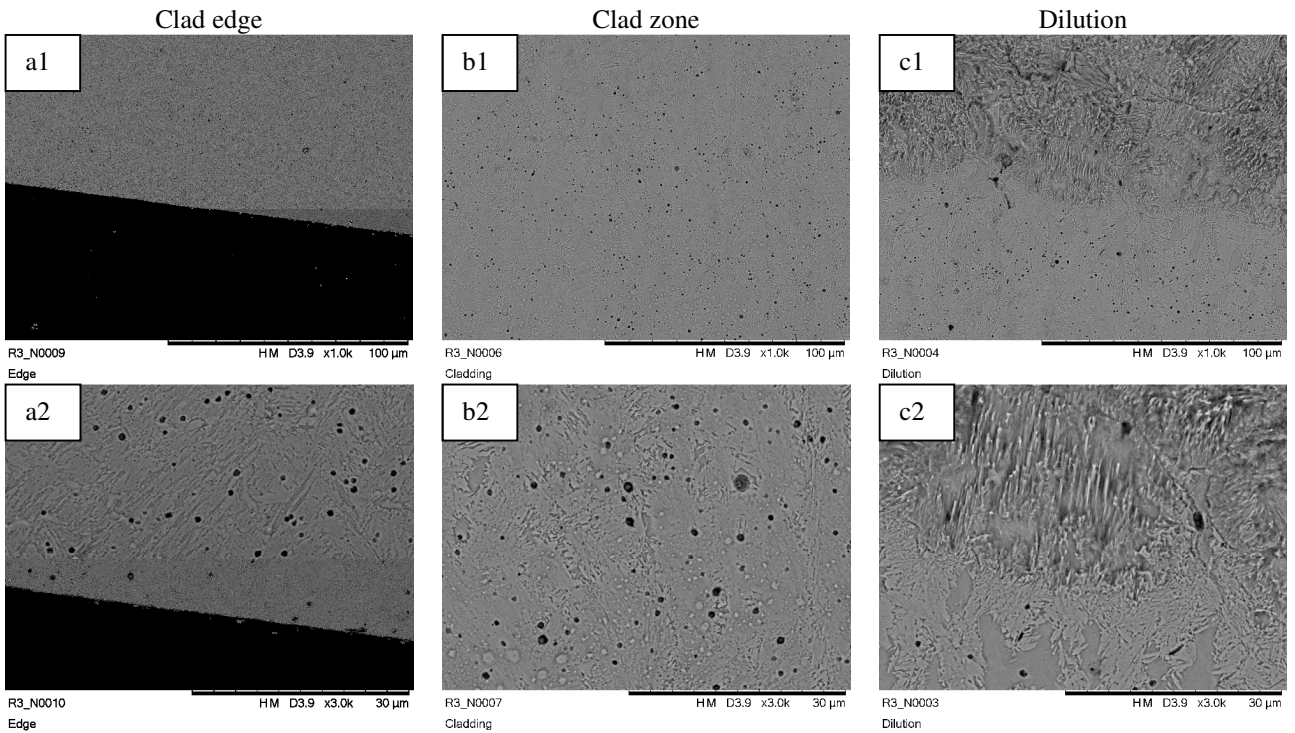


Figure 8. Microstructure of clad zone in untested MMS on R260 (4.76% Nitric, 47.62% hydrochloric and 47.62% water etched): (a1), (a2) are for the clad edge. (b1), (b2) are for the clad zone. (c1), (c2) are for the dilution zone.

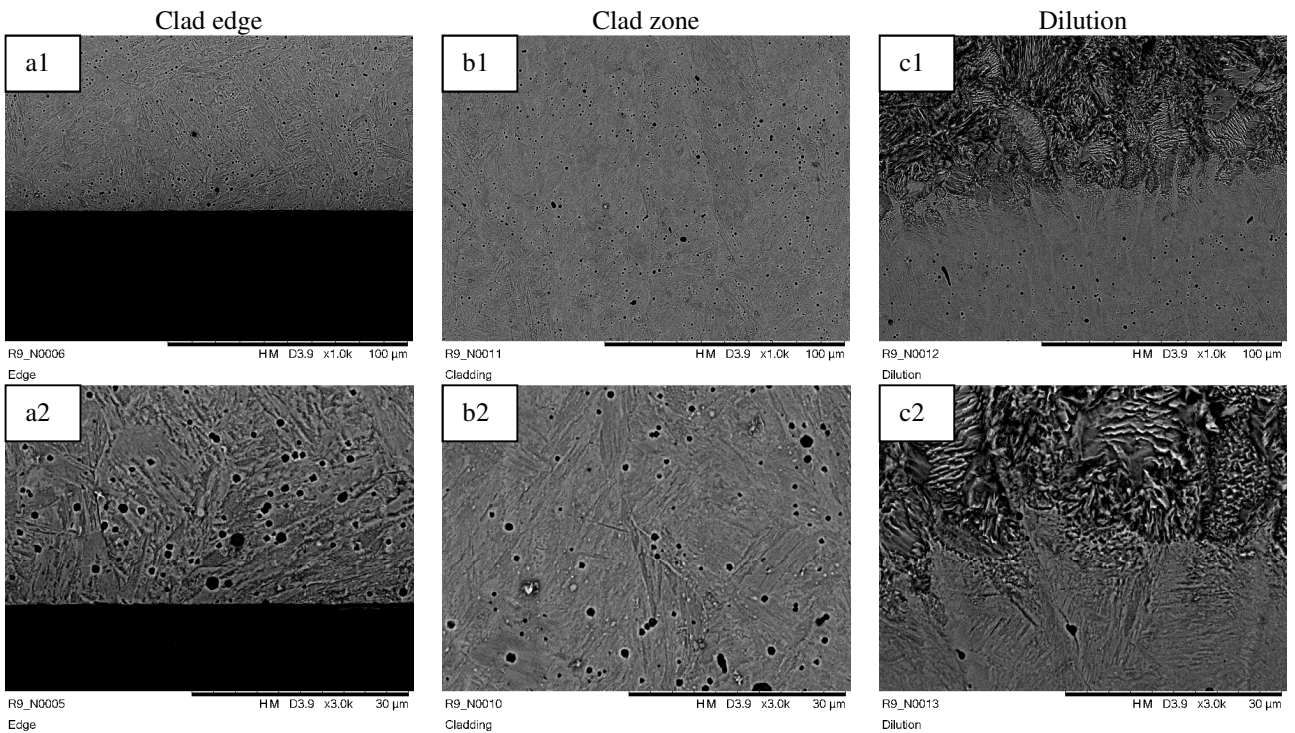


Figure 9. Microstructure of clad zone in untested MMS on R200 (4.76% Nitric, 47.62% hydrochloric and 47.62% water etched): (a1), (a2) are for the clad edge. (b1), (b2) are for the clad zone. (c1), (c2) are for the dilution zone.

Figure 6 (a, b, c) shows the HAZ in the region where full reversion to austenite and subsequent

transformation to lamellar pearlite has occurred during the laser cladding thermal cycle. The coarser grain size adjacent to the cladding/parent material interface is due to the higher temperature experienced at this position. Figure 6 (a1, a2) show the unetched MSS cladding (white), with the dilution zone then showing the first appearance of very fine-structured pearlite colonies. The dilution zone in Figure 6 then changes into a coarse grained (b1, 2) and fine grained (c1, 2), slightly hypo-eutectoid pearlite microstructure, with small ferritic regions embedded amid large pearlitic colonies and grains.

Figure 6 (d, e, f) shows the R260 pearlitic steel microstructure with individual pearlite colonies and grains. Figure 6 (d1, d2) shows the microstructure in the intercritical region. At this location only partial reversion to austenite occurs and the regions which have reaustenitised have transformed to fine lamellar pearlite on cooling. The regions where austenite reversion has not occurred can be seen in Figure 6 (d1, d2) as globular, broken up regions of pearlite; this occurs when the temperature is not sufficiently high for reversion to austenite and the lamellar pearlite begins to break down into the equilibrium constituents for this temperature, i.e., spheroidised cementite particles within a ferrite matrix. The sub-critical HAZ shown in Figure 6 (e1, e2) are comprised mainly of spheroidised pearlite due to the temperature remaining just below the eutectoid temperature of 723°C. However, there are still one or two regions where transformation has occurred as evidenced by the lamellar pearlite in the micrographs. Figure 6 (f1, f2) show the lamellar pearlite structure typical of R260 grade rail; the lamellar being most clearly evident in the higher magnification micrograph of Figure 6 (f2). Figure 6 (d1, e1) also show hardness indents.

A similar microstructure appearance can be seen in Figure 7, with however a more pronounced hypo-eutectoid pearlitic steel substrate of the R200 steel with individual pearlite colonies, separated by larger ferrite grains. This is apparent in all regions in Figure 7 (a-f). R200 has a much lower carbon content than R260 grade rail and as a result the microstructure of the parent rail contains a continuous network of pro-eutectoid ferrite around the prior austenite grain boundaries.

The microstructure of the MMS within the clad zone consisted of a mixture of martensite, retained austenite and delta ferrite for both the deposit on the R200 grade rail and that on the R260 grade rail (Figures 8 and 9). Adjacent to the interface the microstructure of the MMS deposit appeared to contain a higher proportion of blocky austenite, particularly for the deposit on R260 grade rail grade (Figure 8 (c2)). The higher carbon of this rail grade will reduce the amount of delta ferrite and increase the amount of austenite within the microstructure. This was less evident in the deposit adjacent to the interface on the lower carbon R200 grade deposit, although some blocky austenite can be seen (Figure 9 c2).

2.6 Tribological testing

Testing was conducted using the SUROS twin-disc testing machine shown in Figure 1, taking the 47mm diameter wheel and rail discs and loading them to produce a small-scale contact capturing the key elements of combined rolling-sliding behaviour characteristic of a rail-wheel contact. With a line contact length in the lateral dimension of wheel/rail rollers of 10 mm, contact load of 7.14 kN which gives a maximum Hertzian contact pressure of 1500 MPa. A rail disc rotational speed of 400 rpm and creep of 1% was also used representing a driving wheel condition. Wear tests were conducted under dry conditions. During the wear testing the tests were stopped every 5,000 cycles so that the evolution of the wear rate could be measured. These are standard wear settings for SUROS testing [19].

Material loss was measured in the tests with microstructural analysis. Microhardness measurements of the specimens was carried out before and after testing to investigate what effect the substrate grade had on the performance of the clad MSS deposit. Comparisons were also made to baseline measurements for R200 and R260.

3. Results & Discussion

3.1 Wear behaviour

Figure 10 shows the evolution of the wear rates of the rail and wheel discs. All tests depicted in this section were conducted under dry contact condition with a maximum Hertzian contact pressure of 1500 MPa and 1

% creep. These results were also compared with tests done under identical conditions in [8].

Two groups of test were conducted with the MSS R260 and MSS R200 samples, one set with compressed air jet spraying on samples for temperature control during tests, and one set without the cooling air. The results have been compared with the results from Lewis et al. [8], in which tests were done with cooling air. With the cooling air, the contact temperature between discs were kept at $37 \pm 1^\circ\text{C}$ during the whole test.

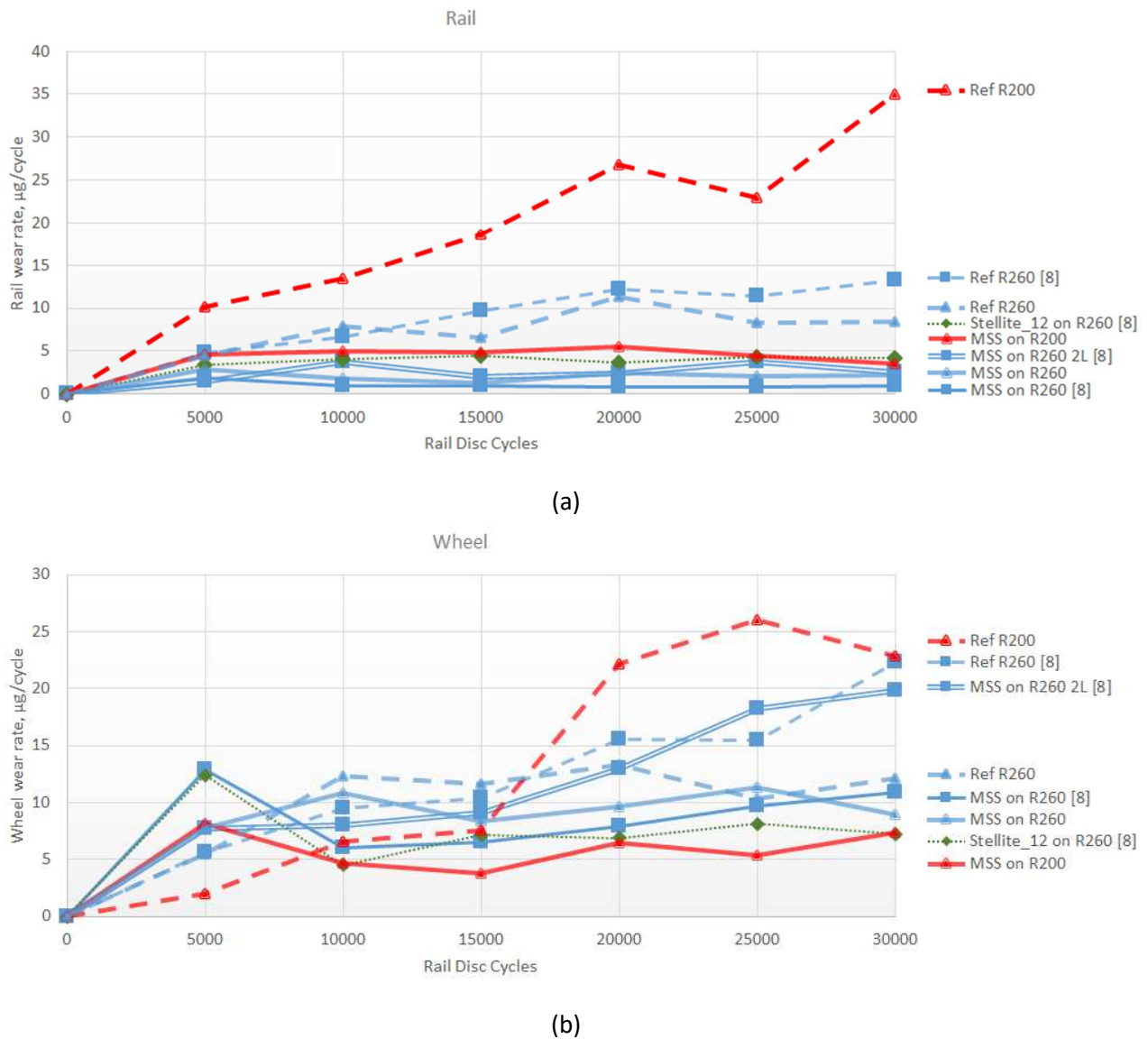


Figure 10. Wear rate evolution of (a) the rail discs and (b) the wheel discs with the number of test cycles for the R200 clad with MSS and R260 clad with MSS. The chart includes data from [8] with various material deposited onto R260 material. All tests were performed under identical conditions. 1L indicates 1 layer and 2L indicates a 2-layer sample. All samples tested in the work reported in this paper were made with 1 layer.

From Figure 10 (a), it can be seen that the MSS on R200 and MSS on R260 rail discs wore at similar rates and had similar performance to an R260 disc clad with Stellite 12 and MSS tested in previous work [8]. It is encouraging that an MSS clad layer on a lower grade of rail steel is still giving a good improvement in wear resistance over the R260 baseline. Even though, as Figure 5 demonstrates, its hardness directly after cladding, was affected. Interestingly the post-test surface hardness of the MSS 1L tested in [8] was 766HV compared to 630 HV for the MSS clad on R260 sample tested here (see Figure 5). It must also be noted though that the 1 layer samples tested in this work wore more than the 1 layer MSS sample tested in [8]. There are a few potential explanations for this: a) that the powder and hence the eventual deposited MSS

was from a different batch for the tests reported in this paper as compared to the samples in [8]. Also, in this work, whole cylinders of R200 and R260 material were clad and then manufactured into SUROS samples. In [8] the SUROS samples were first machined and then individually clad. This latter approach caused issues with heat dissipation during the cladding process and very high cooling rates of the clad were observed. The tests without cooling air applied did not differ from those without so are not shown.

Table 2 summarises the wear rate of all the rail specimens shown in Figure 10 averaged over the whole 30,000 cycle test period. In Table 2 any wear rate which was in excess of either the Reference (R260 Grade) wheel or rail, i.e. 100% or greater, has been highlighted in red. Any wear rate which is less than the reference is highlighted green indicating good wear performance. Wear rates which are less than 50% of the reference case are highlighted light green indicating superior wear performance.

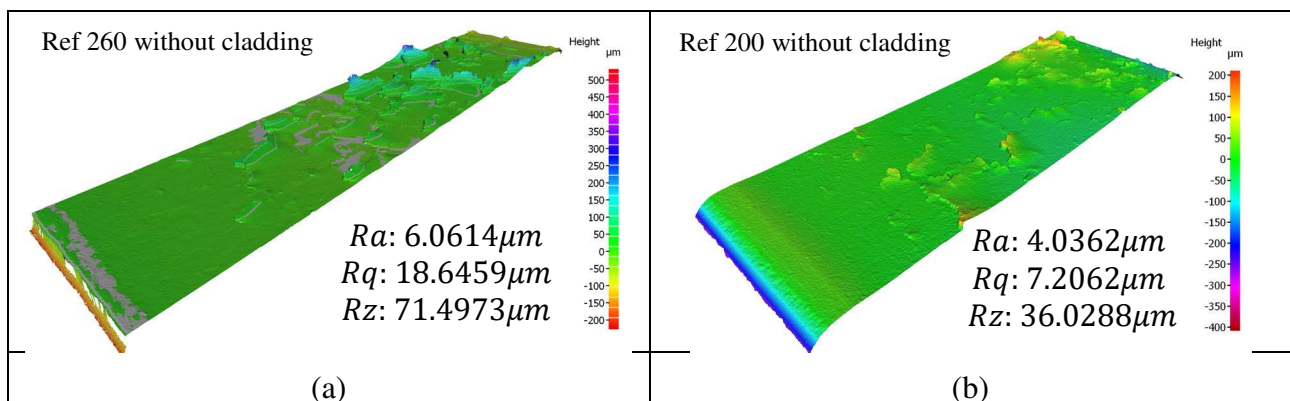
It should be noted that the wear rates of the reference tests in [8] were slightly higher (both wheel and rail by approximately 20%) than the current reference tests. It can be seen from Table 2 that all of the clad rail discs tested are in the good/ superior wear category. The MSS on R260 rail discs have shown superior wear resistance, which gave a 65%-73% wear rate reduction. Even the MSS on R200 rail discs have presented a 40% wear rate reduction compared to the standard R260 samples. At the same time, the wear rate of corresponding wheel discs also fell within the good wear category.

Table 2. Averaged wear rates of rail specimens over the entire 30,000 cycles (Data from similar tests performed in [8] included for comparison).

Clad	Wear Rate		Wear Rate	
	$\mu\text{g}/\text{cycle}$		Percentage of 260 Ref	
	W	R	W	R
Ref R260	10.88	7.84	100%	100%
Ref R200	14.52	21.13	133%	270%
Ref R260 [8]	13.14	9.64	121%	123%
MSS R200	5.97	4.62	55%	59%
MSS R260	9.49	2.11	87%	27%
MSS_1L R260 [8]	8.96	1.04	82%	13%
MSS_2L R260 [8]	12.65	2.63	116%	34%
Stellite12_1L R260 [8]	7.72	4	71%	51%

3.2 Topography measurements

All surfaces were examined using the optical (non-contact) Alicona Infinite-Focus SL profilometer (Alicona Imagine GmbH, Raaba, Austria) after 30000 cycles, producing high-resolution images and 3D surface profiles measurements with a vertical resolution of up to 10 nm.



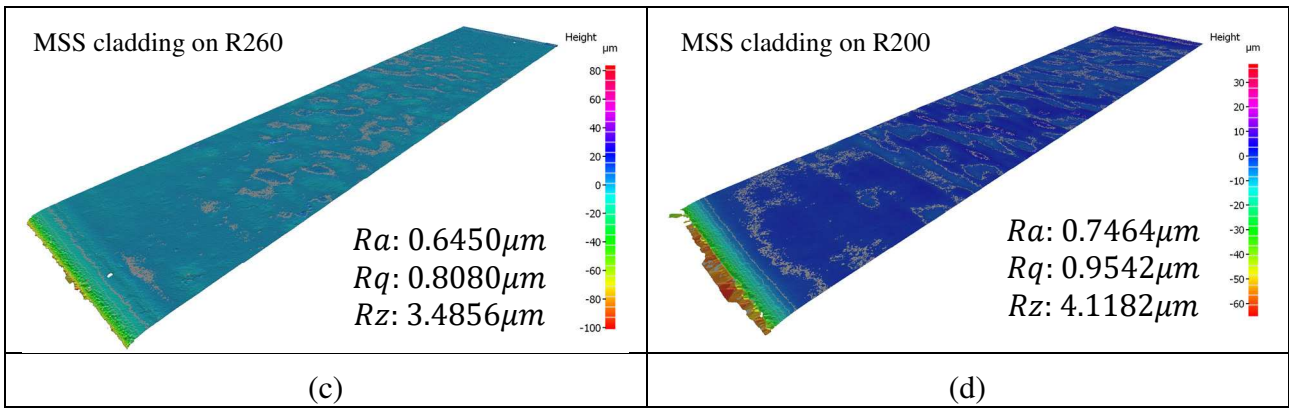


Figure 11. Topography measurements of tested samples.

As can be seen from Figure 11, both MSS on R260 and MSS on R200 specimens have shown a smooth surface finish after tests, with a surface roughness $R_a < 0.75\mu m$. This indicates that only mild wear occurred during tests, and these smooth surfaces show no sign of flake formation characteristic of a significant depth of material reaching the ductility exhaustion strain at which large flakes would form. In contrast, on the reference R260 rail disc it can be observed that the top layer of material was peeling up from the surfaces, and the surface roughness was 10 times higher than that of the cladded specimens. This suggests that strain in the surface has accumulated (i.e. by a ratchetting mechanism) to the point of ductility exhaustion at which it loses integrity and breaks away from the main body of the steel.

3.3 Sub-surface inspection

After the surface topography measurements, tested rail specimens were then sectioned and examined for: micro hardness and micro- structural changes. The specimens were sectioned in the radial direction, as indicated in Figure 12 (a). The 2% Nital etched cross-sections from the tested samples are shown in Figure 12 (b), (c), (d) and (e). Clearly deformation can be observed with the non-clad specimens, Figure 12 (b) and (d), where the edge was squeezed out of the contact. The subsurface microstructure in the middle zone was heavily compressed, while the microstructure at the edge remained the same with the original substrate, which indicates the deformation happened in the early stage of wear tests. For the clad specimens, Figure 12 (c) and (e), only minimum deformation occurred. It should be noted that for the MSS on R260 specimen, the edges were chamfered rather than worn out.

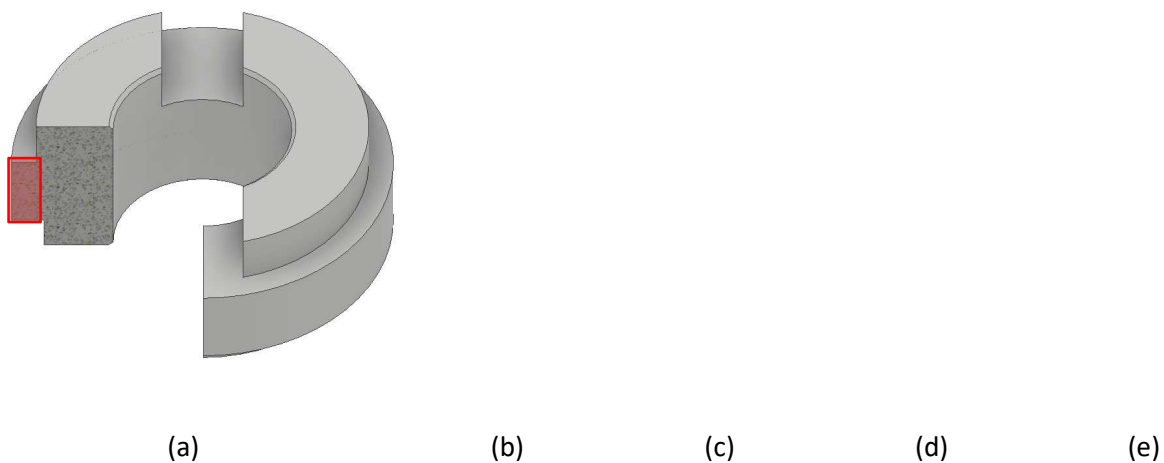
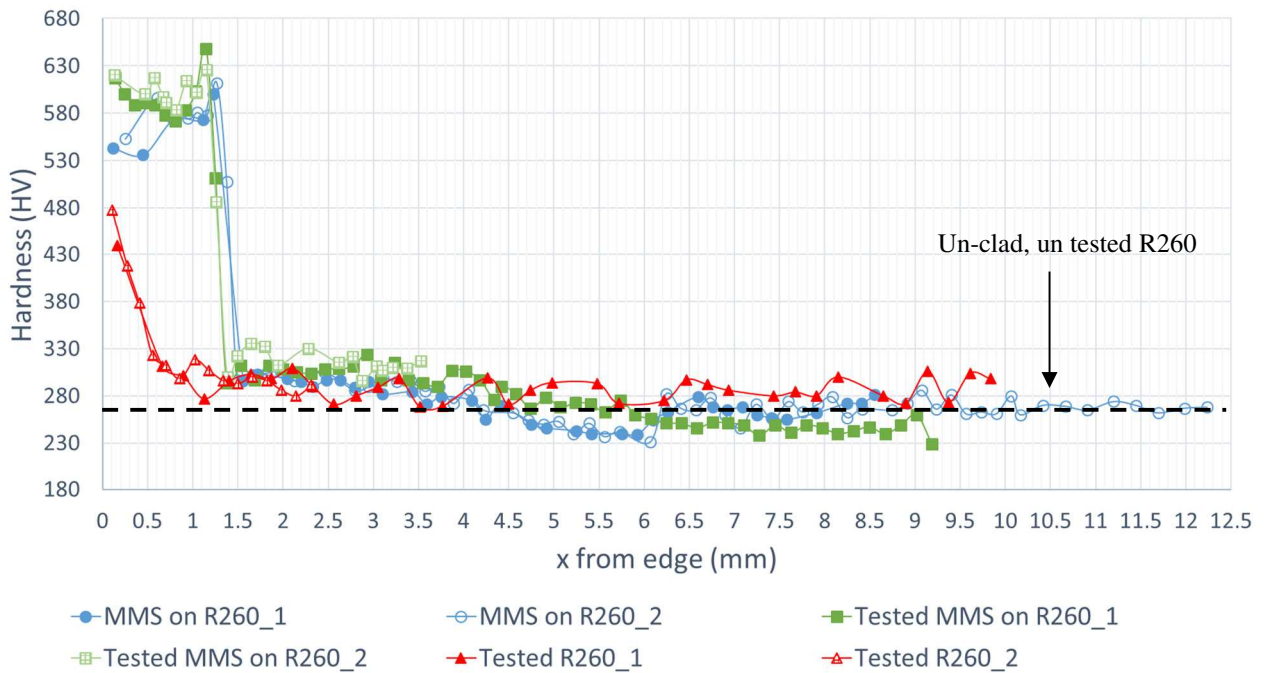


Figure 12. Cross-section deformation of SUROS discs (a) Section view, (b) R260, (c) MSS on R260, (d) R200 and (e) MSS on R200.

Figure 13 gives a comparison of the hardness pre and post testing. The average hardness profile of the

tested-specimens' cross-section in Figure 13 demonstrates the effective depth of plastic deformation. It should be noted that these hardness values were gathered from different specimens, but all were taken from the same parent material. As can be seen from the hardness measurements shown in Figure 13, the outside layer of both non-clad materials were worked hardened during tests. For the non-clad R260 sample, the bulk hardness was reached at about 0.7 mm from the surface. The maximum hardness, roughly 480 HV, was measured from the sub-surface region. For the non-clad R200 sample, a maximum hardness of around 530 HV was achieved near the top surface, and the maximum work hardened depth was around 1.1 mm. For the cladded rail specimens, the work-hardened effects were not as marked as for the reference non-clad samples.



(a)

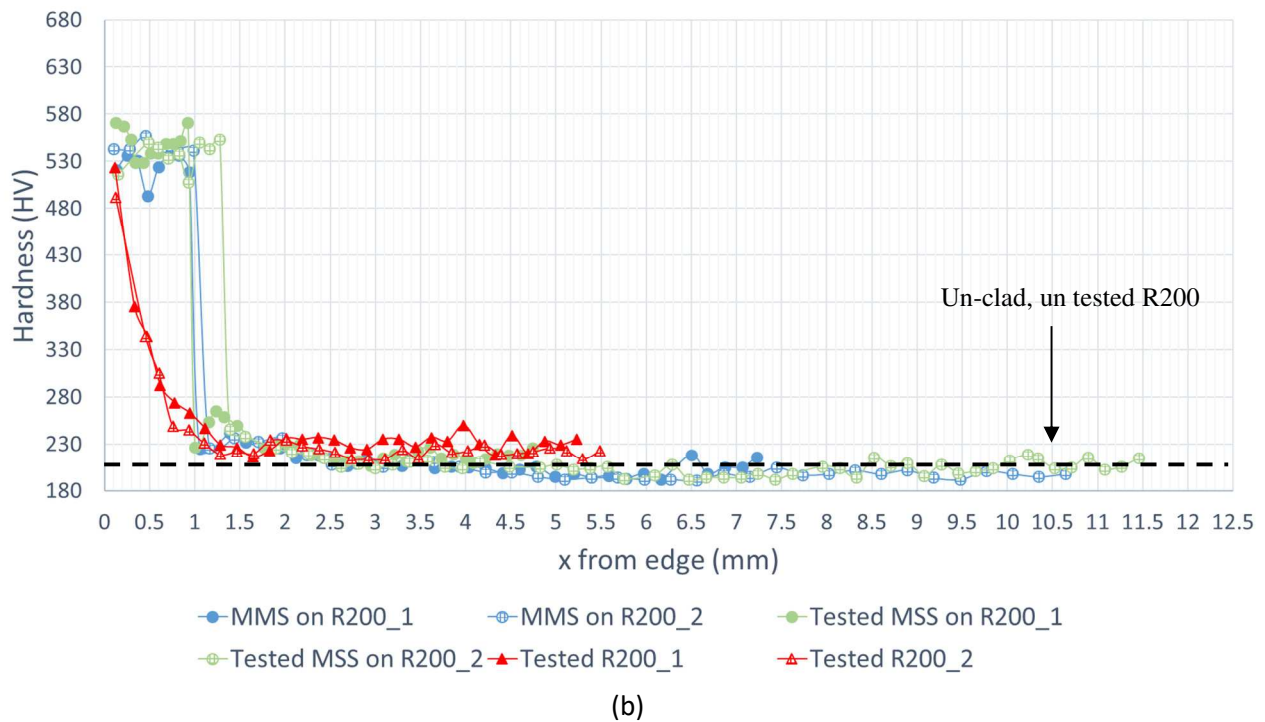


Figure 13. Microhardness measurements for the (a) MSS clad on R200 and tested reference R200 sample
 (b) MSS clad on R260 and tested reference R260 sample
 with the straight line representing the mean microhardness of standard un-clad, un-tested rail material.
 All measurements were performed with a load of 1kg.

To get a more accurate measurement of the depth of deformation, the sub-section of samples was examined under SEM. According to measurements judged by visual observation, see Figure 14 (b) and (c), the clad rail samples had a deformation depth of 10 and 20 μm . Only a very thin layer of the MSS clad layer shows material flow, and no cracks could be observed within this deformation layer, i.e. the material had not reached its ductility limit under the prevailing ratchetting conditions. The rest of the clad layer had the same structure as the untested samples shown in Figure 7 and Figure 8. The low amount of plastic deformation in the clad rail specimens also explains why no cracks were seen in all of the clad rail specimens.



- wheel/rail materials," *Proceedings of the Institution of Mechanical Engineers, Part J: Journal of Engineering Tribology*, vol. 228, no. 1, pp. 114-122, 2014/01/01 2013.
- [7] W. J. Wang, J. Hu, J. Guo, Q. Y. Liu, and M. H. Zhu, "Effect of laser cladding on wear and damage behaviors of heavy-haul wheel/rail materials," *Wear*, vol. 311, no. 1, pp. 130-136, 2014/03/15/ 2014.
- [8] S. R. Lewis *et al.*, "Improving rail wear and RCF performance using laser cladding," *Wear*, vol. 366-367, pp. 268-278, 2016/11/15/ 2016.
- [9] S. Jalili Hassankiadeh, "Failure analysis of railway switches and crossings for the purpose of preventive maintenance," ed, 2011.
- [10] W.-J. Zwanenburg, "Modelling degradation processes of switches & crossings for maintenance & renewal planning on the Swiss railway network," 2009.
- [11] C. Guo *et al.*, "Effects of WC–Ni content on microstructure and wear resistance of laser cladding Ni-based alloys coating," *Surface and Coatings Technology*, vol. 206, no. 8, pp. 2064-2071, 2012/01/15/ 2012.
- [12] H.-m. Guo, Q. Wang, W.-j. Wang, J. Guo, Q.-y. Liu, and M.-h. Zhu, "Investigation on wear and damage performance of laser cladding Co-based alloy on single wheel or rail material," *Wear*, vol. 328-329, pp. 329-337, 2015/04/15/ 2015.
- [13] W. J. Wang, Z. K. Fu, X. Cao, J. Guo, Q. Y. Liu, and M. H. Zhu, "The role of lanthanum oxide on wear and contact fatigue damage resistance of laser cladding Fe-based alloy coating under oil lubrication condition," *Tribology International*, vol. 94, pp. 470-478, 2016/02/01/ 2016.
- [14] S. R. Lewis *et al.*, "Full-scale testing of laser clad railway track; Case study – Testing for wear, bend fatigue and insulated block joint lipping integrity," *Wear*, vol. 376-377, pp. 1930-1937, 2017/04/15/ 2017.
- [15] Z. K. Fu, H. H. Ding, W. J. Wang, Q. Y. Liu, J. Guo, and M. H. Zhu, "Investigation on microstructure and wear characteristic of laser cladding Fe-based alloy on wheel/rail materials," *Wear*, vol. 330-331, pp. 592-599, 2015/05/01/ 2015.
- [16] S. R. Lewis, R. Lewis, and D. I. Fletcher, "Assessment of laser cladding as an option for repairing/enhancing rails," *Wear*, vol. 330-331, pp. 581-591, 2015/05/01/ 2015.
- [17] J.-m. Chen, C. Guo, and J.-s. Zhou, "Microstructure and tribological properties of laser cladding Fe-based coating on pure Ti substrate," *Transactions of Nonferrous Metals Society of China*, vol. 22, no. 9, pp. 2171-2178, 2012/09/01/ 2012.
- [18] P. Beaty, B. Temple, M. B. Marshall, and R. Lewis, "Experimental modelling of lipping in insulated rail joints and investigation of rail head material improvements," *Proceedings of the Institution of Mechanical Engineers, Part F: Journal of Rail and Rapid Transit*, vol. 230, no. 4, pp. 1375-1387, 2016/05/01 2015.
- [19] D. Fletcher and J. Beynon, "Development of a Machine for Closely Controlled Rolling Contact Fatigue and Wear Testing," 2000.
- [20] B. Dahl, B. Mogard, B. Greftoft, and B. Ulander, "Repair of rails on-site by welding," *Swedish National Rail, SE-781*, vol. 85, 1995.
- [21] D. Farichild, N. Bangaru, J. Koo, P. Harrison, and A. Ozekcin, "A study concerning intercritical HAZ microstructure and toughness in HSLA steels," *Welding Journal*, vol. 70, no. 12, pp. 321. s-329. s, 1991.